Minireview

# Protonmotive force generation by a redox loop mechanism

Mika Jormakka[a,*], Bernadette Byrne[b], So Iwata[a,b,*]

[a] *Division of Biomedical Sciences, Imperial College London, London SW7 2AZ, UK*
[b] *Department of Biological Sciences, Imperial College London, London SW7 2AZ, UK*

Received 18 February 2003; accepted 24 February 2003

First published online 22 April 2003

Edited by Bernard L. Trumpower

**Abstract Respiration involves the oxidation and reduction of substrate for the redox-linked formation of a protonmotive force (PMF) across the inner membrane of mitochondria or the plasma membrane of bacteria. A mechanism for PMF generation was first suggested by Mitchell in his chemiosmotic theory. In the original formulations of the theory, Mitchell envisaged that proton translocation was driven by a 'redox loop' between two catalytically distinct enzyme complexes. Experimental data have shown that this redox loop does not operate in mitochondria, but has been confirmed as an important mechanism in bacteria. The nitrate respiratory pathway in *Escherichia coli* is a paradigm for a protonmotive redox loop. The structure of one of the enzymes in this two-component system, formate dehydrogenase-N, has revealed the structural basis for the PMF generation by the redox loop mechanism and this forms the basis of this review.**


*Key words:* Protonmotive force; Nitrate respiration; Redox loop; Chemiosmotic theory

## 1. Introduction

The respiratory electron transport chain (ETC) present in the inner membrane of mitochondria and in the cytoplasmic membrane of prokaryotes converts energy derived from redox reactions into a protonmotive force ($\Delta p$, or PMF) across the membrane [1,2]. The PMF has two components: the electrochemical gradient ($\Delta\psi$), and the concentration difference of protons ($\Delta$pH) across the membrane. The cell uses the PMF to drive both the synthesis of ATP (adenosine 5′-triphosphate) from ADP (adenosine 5′-diphosphate) and substrate transport. Given the central role of electron transport in these processes, a considerable amount of research has focused on attempting to explain the precise molecular mechanism behind the generation of PMF.

*Corresponding authors. Fax: (44)-20-7594 3022.
*E-mail addresses:* mika.jormakka@imperial.ac.uk (M. Jormakka), b.byrne@imperial.ac.uk (B. Byrne), s.iwata@imperial.ac.uk (S. Iwata).

*Abbreviations:* ADP, adenosine 5′-diphosphate; ATP, adenosine 5′-triphosphate; *bis*-MGD, *bis*-molybdopterin guanine dinucleotide; ETC, electron transport chain; Fdh-N, formate dehydrogenase-N; HOQNO, 2-heptyl-4-hydroxyquinoline-*N*-oxide; NADH, reduced nicotinamide adenine dinucleotide; Nar, nitrate reductase; PMF, protonmotive force; SeCys, selenocysteine

In Mitchell's original mechanistic explanation of the chemiosmotic theory, he described the oxygen respiratory chain as a series of *redox loops* between the respiratory enzymes in the membrane, where electrons were transferred from the outside to the inside of the membrane and then co-transported back across the membrane with protons, in the form of quinol [2]. Redox loops are found in pathways involving enzymes, which contain the active sites for the substrate and the quinone on opposite sides of the membrane. By this arrangement, chemical or scalar protons are produced and consumed on opposite sides of the membrane. These early theories were later modified by the addition of the more complex mechanisms of the Q-cycle for the ubiquinol–cytochrome *c* oxidoreductase (cyt $bc_1$ complex), and proton pumping by reduced nicotinamide adenine dinucleotide (NADH):ubiquinone oxidoreductase (Complex I) and cytochrome *c* oxidase (Complex IV). A combination of these mechanisms has been shown to generate the PMF when molecular oxygen is the terminal electron acceptor.

During oxidative phosphorylation, the generation of a PMF across the inner membrane of mitochondria and bacterial species is mediated via a series of membrane-bound enzyme complexes (Complexes I–IV). These respiratory enzymes form an ETC and use the release of free energy by the oxidation of substrates to pump protons against the membrane potential. The electrons are generated from the substrate NADH and succinate, produced by the oxidation of glucose via glycolysis and the Krebs cycle. Oxidation of NADH by Complex I and succinate by Complex II (succinate:ubiquinone oxidoreductase), releases electrons that are transferred through redox centers and via quinone through the ETC and finally reduce molecular oxygen to water. The subsequent flow of protons back across the membrane via ATP synthase releases free energy for the production of ubiquitous ATP from ADP and phosphate. The crystal structures of three of the complexes (II–IV) [3–6] in the ETC and $F_1$ ATPase [7] together with biochemical data have provided details of how these proteins cooperate to generate a PMF. In oxidative phosphorylation, the redox loop originally formulated in Mitchell's chemiosmotic theory is not operational, although there are similarities in the loops formed between Complex I/II and the cyt $bc_1$ complex (Complex III) as well as in the Q-cycle [8].

## 2. Flexibility in prokaryotes enables them to induce alternative respiratory pathways depending on environmental factors

In addition to oxidative phosphorylation, most prokaryotes

0014-5793/03/$22.00 © 2003 Published by Elsevier Science B.V. on behalf of the Federation of European Biochemical Societies.
doi:10.1016/S0014-5793(03)00389-2

have the ability to use alternative, inducible respiratory pathways utilizing terminal electron acceptors other than molecular oxygen. In anaerobic environments the diverse range of electron acceptors includes sulfur, nitrogen, selenium, and transition metals such as Fe(III) and Mn(IV) [9,10]. Environmental factors determine the respiratory pathway induced, and since the $H^+/e^-$ ratios differ for the enzymes, this variability has consequences for energy conservation [10]. One major alternative respiratory pathway is the nitrate respiratory pathway, which is induced by anaerobiosis and the presence of nitrate [11]. Under these conditions the production of two energy-yielding enzymes is induced: formate dehydroge-

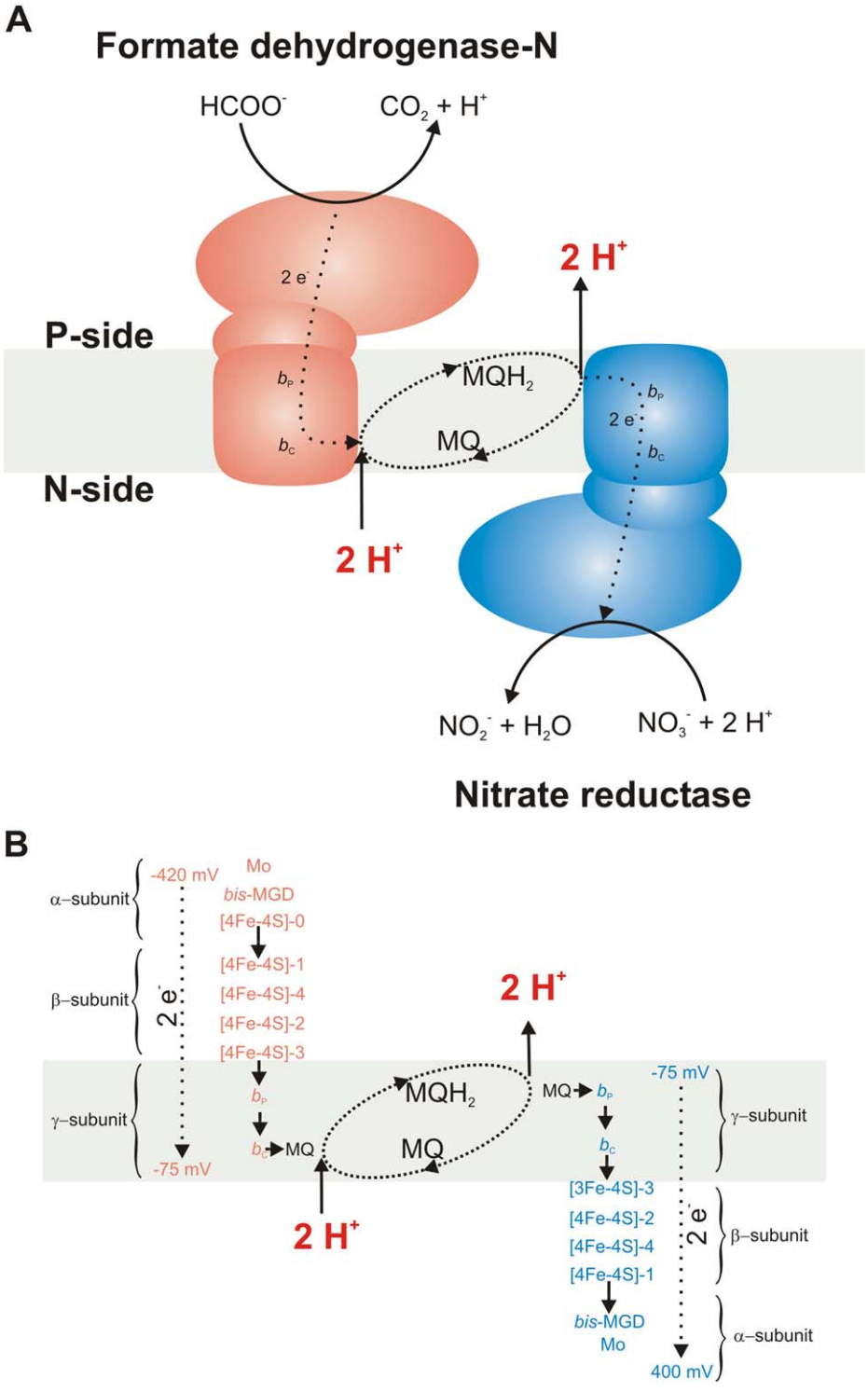


Fig. 1. The nitrate respiratory pathway. A: Fdh-N is illustrated in red and Nar in blue. The substrate and menaquinone binding sites of the enzymes are situated on opposite sides of the membrane, enabling PMF generation via the redox loop mechanism. Electrons are transferred from the formate oxidation site in the periplasm to the nitrate reduction site situated on the cytoplasmic space of Nar. Menaquinone couples these two reactions and translocates two $H^+$ from the N-side to the P-side, generating PMF. In panel B, the redox centers and potential of the system are illustrated. The highly exergonic reaction allows electrons to be transferred against the membrane potential.

nase-N (Fdh-N) and dissimilatory nitrate reductase (Nar). These two cooperate in generating a PMF through the redox loop mechanism by utilizing the electrons from substrate (formate) oxidation and reduction of nitrate coupled by the lipid mobile electron carrier menaquinone (Fig. 1).

## 3. Example of a redox loop: the nitrate respiratory pathway

The nitrate respiratory pathway, best characterized in *Escherichia coli* and *Paracoccus denitrificans* [12–14], consists of Fdh-N and Nar, members of an enzyme family binding the *bis*-molybdopterin guanine dinucleotide (*bis*-MDG) cofactor in their active site [15]. In the absence of oxygen and in the presence of nitrate, these enzymes serve as oxidoreductases to provide energy for the bacterial cells.

Both Fdh-N and Nar are membrane-bound heterotrimeric enzymes that contain *bis*-MGD cofactor, heme, and non-heme iron. Additionally Fdh-N is one of only three *E. coli* proteins that contain intrinsic selenocysteine (SeCys) [12,16]. Purified Fdh-N and Nar consist of two membrane-associated domains and an integral membrane domain. All three subunits of Fdh-N are coded for by the FdnGHI operon. The α-subunit (FdnG) is a membrane-associated subunit, incorporating a SeCys residue and a [4Fe–4S] cluster in addition to *bis*-MGD cofactor [17]. The β-subunit (FdnH) is another membrane-associated subunit which contains four [4Fe–4S] clusters and one transmembrane helix. The γ-subunit (FdnI) is the integral membrane subunit, which anchors the other two subunits to the membrane. It also incorporates two heme *b* groups and a menaquinone binding site. Similarly, the NarGHI operon codes for the three subunits of Nar. NarG and NarH code for the membrane-associated subunits, which bind *bis*-MGD cofactors and four iron–sulphur clusters (FeS), respectively. The product of NarI in the integral membrane subunit contains two heme *b* groups and a menaquinol oxidation site.

In this system, formate is oxidized on the periplasmic side of Fdh-N to $CO_2$ and $H^+$, releasing two electrons that are transferred across the membrane to a bound menaquinone, which upon reduction takes up two protons from the cytoplasm. The formed menaquinol then diffuses across the membrane to the quinol oxidation site on the periplasmic side of Nar, releasing the protons to the periplasm and transferring the electrons to the nitrate reduction site on the cytoplasmic side of the membrane. Here, nitrate is reduced to nitrite, consuming two cytoplasmic protons. Energy is conserved in this system by the net movement of negative charge across the membrane as well as a net movement of protons [15]. This model is supported by the analysis of proton movements in spheroplasts in response to nitrate reduction when electron donors that input electrons to Nar on different sides of the membrane are employed [18–20].

## 4. Crystal structure of Fdh-N complex provides insight into PMF generation by the redox loop mechanism

Proof of the redox loop mechanism in this system came in the form of the crystal structure of the oxidized form of Fdh-N (PDB entry 1KQF) [21]. The high resolution (1.6 Å) of this structure provided detailed insight into the electron transfer pathway, and the topology and placement of the redox centers has successfully explained how this system generates a PMF via the redox loop mechanism. The structure revealed that the catalytic α-subunit is situated on the periplasmic side of the membrane, while biochemical data strongly suggest that the equivalent subunit of Nar is located on the cytoplasmic side of the membrane. As stated earlier, this opposite directionality is the key to energy-efficient PMF generation by the redox loop mechanism.

### 4.1. Fdh-N; overall composition and redox centers

The redox centers of Fdh-N are aligned almost linearly from the *bis*-MGD cofactor of the catalytic site, through the single [4Fe–4S] cluster in the α-subunit and the four [4Fe–4S] clusters in the β-subunit, and finally the two heme *b* groups in the integral membrane γ-subunit. The overall structure and redox centers of Fdh-N are shown in Fig. 2. The catalytic α-subunit has a similar overall structure and position of its prosthetic groups as the other related *bis*-MGD enzymes with known structure. These include a periplasmic Nar from *Desulfovibrio desulfuricans* [22], and Fdh-H from *E. coli* [23], which is part of the formate hydrogenlyase complex. The structure of Fdh-N shows how the catalytic site Mo-atom is coordinated by the *cis*-thiolate groups of the *bis*-MGD cofactors as well as directly to the intrinsic SeCys. The β-subunit is anchored to the membrane with a single transmembrane α-helix and contains four [4Fe–4S] clusters arranged in two pairs. The integral membrane γ-subunit is composed of four transmembrane helices, coordinating two heme *b* groups situated on opposite sides of and perpendicular to the membrane normal.

### 4.2. Electron transfer in Fdh-N

In this first half of a redox loop, electrons are transferred from formate in the α-subunit to menaquinone in the γ-subunit. The electron transfer from formate (standard redox potential, −420 mV) to menaquinone (−75 mV) is a highly exergonic reaction, allowing the transfer of two electrons against the membrane potential, and the subsequent generation of a proton gradient. In Fdh-N, edge-to-edge distances between the redox centers are in the range from 6 to 11 Å, which is shorter than the reported 14 Å limit of physiological electron transfer [24]. The shortest distance between metal centers between two adjacent monomers is 26.5 Å, indicating that electron transfer only occurs within the monomer and that the monomer is the functional unit of the enzyme, despite the formation of the physiological trimer.

In the catalytic site, situated in the periplasmic space, electrons are transferred directly from the substrate to the Mo-cofactor [23]. The electrons released there are transferred to the β-subunit though the [4Fe–4S] cluster (FeS-0) in the α-subunit. In the β-subunit, electrons are transferred through four [4Fe–4S] clusters in the order of FeS-1, FeS-4, FeS-2 and FeS-3. The structure of Fdh-N showed that the coordination pattern of the [4Fe–4S] clusters in the β-subunit is the same as predicted for Nar by mutation analysis [25,26]. This information, together with sequence analysis, shows that Nar and Fdh-N have very similar α- and β-subunits, indicating a similar electron transport mechanism, although with reverse electron flows. No measurements of the redox potentials of the Fdh-N [4Fe–4S] clusters have been made, although the corresponding clusters in Nar have been studied. These studies have shown that there is a large variation between the redox potentials of the iron–sulfur clusters (+130, −420,

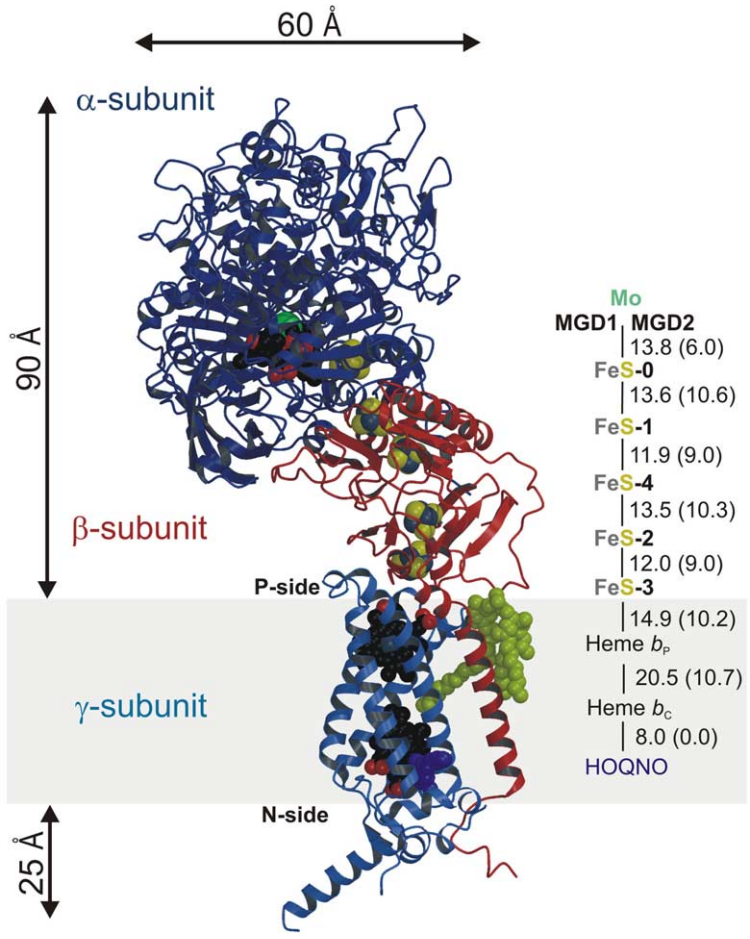


Fig. 2. A monomer of Fdh-N viewed from the plane of the membrane. The catalytic α-subunit is shown in dark blue, the electron transfer β-subunit in red and the membrane intrinsic γ-subunit in marine. The *bis*-MGD cofactor as well as the two heme *b* molecules are shown in black (oxygen in red), with the active site Mo atom in green. Iron atoms in the iron–sulfur clusters are colored gray while sulfur and cardiolipin are shown in yellow. HOQNO is shown in purple. Also illustrated is the electron transfer pathway, which is linear and spanning close to 90 Å from Mo to the quinone binding site. Center-to-center and edge-to-edge (parentheses) distances between the redox centers are shown. This figure was made using MOLSCRIPT [34] and rendered using RASTER3D [35].

−55 and +180 mV for clusters 1, 4, 2 and 3, respectively) [25], which could be explained by the observation that the Fdh-N clusters 2 and 4 are hydrogen-bonded by several positively charged residues [21]. From FeS-3, electrons are transferred to heme $b_P$ in the γ-subunit, then across the membrane to heme $b_C$ against the membrane potential.

### 4.3. 2-Heptyl-4-hydroxyquinoline-N-oxide (HOQNO) binding site and possible proton uptake channel

In addition to the native structure, the structure of Fdh-N with bound quinone inhibitor was obtained (PDB entry 1KQG). Quinone requirement for the Fdh-N/Nar system has been demonstrated in studies by Taniguchi et al. [27], who found that HOQNO inhibited formate–nitrate oxidoreductase activity, but had little or no effect on reduced methylene-blue–nitrate oxidoreductase activity. This was later confirmed by Enoch and Lester [28], working with purified preparations of Fdh-N and Nar. The menasemiquinone analog HOQNO was successfully used for soaking into Fdh-N crystals and the resultant 2.8 Å structure revealed the quinone reduction site at the cytoplasmic side of the membrane, placing the active sites for formate and quinone on opposite sides of the membrane. Furthermore, a possible solvent chain leading out to the cytoplasm from the reduction site has been identified. This would allow reduced quinol to receive protons from the cytoplasm, consistent with the chemiosmotic theory.

The binding pocket is formed by residues from two transmembrane helices ($tm^{\gamma}$ II and $tm^{\gamma}$ III) and the loop region between them (Fig. 3A). In the inhibitor structure, the *N*-oxide group of HOQNO (homologous to $O_1$ of menaquinone) forms a hydrogen bond with $His^{\gamma169}$, a heme $b_C$ ligand. This is the first example where the heme ligand is directly involved in quinone binding. The ligand for the OH group of HOQNO (homologous to $O_4$ of menaquinone) is less clear, although a water molecule (w1990) has been suggested to be a direct ligand. The $N_\varepsilon$ atom of $Asn^{\gamma110}$ was also suggested to be a possible ligand, although the CO–N angle (85°) is not suitable for stable hydrogen-bond formation. A mutant of the equivalent residue to $Asn^{\gamma110}$ ($Asn^{128} \rightarrow Asp$) of *Wollinera succinogenes* [NiFe] hydrogenase, shows less than 10% quinone reduction activity compared to the wild type [29]. This shows that the residue is important for the menaquinone binding, although it may not act as a direct ligand.

In the published native structure, a water molecule (w1990) is connected to the cytoplasmic space via a water chain, maintained by hydrogen bonds to polar residues including $Glu^{\gamma100}$ and $His^{\gamma197}$ and one propionate from heme $b_C$. In the presence

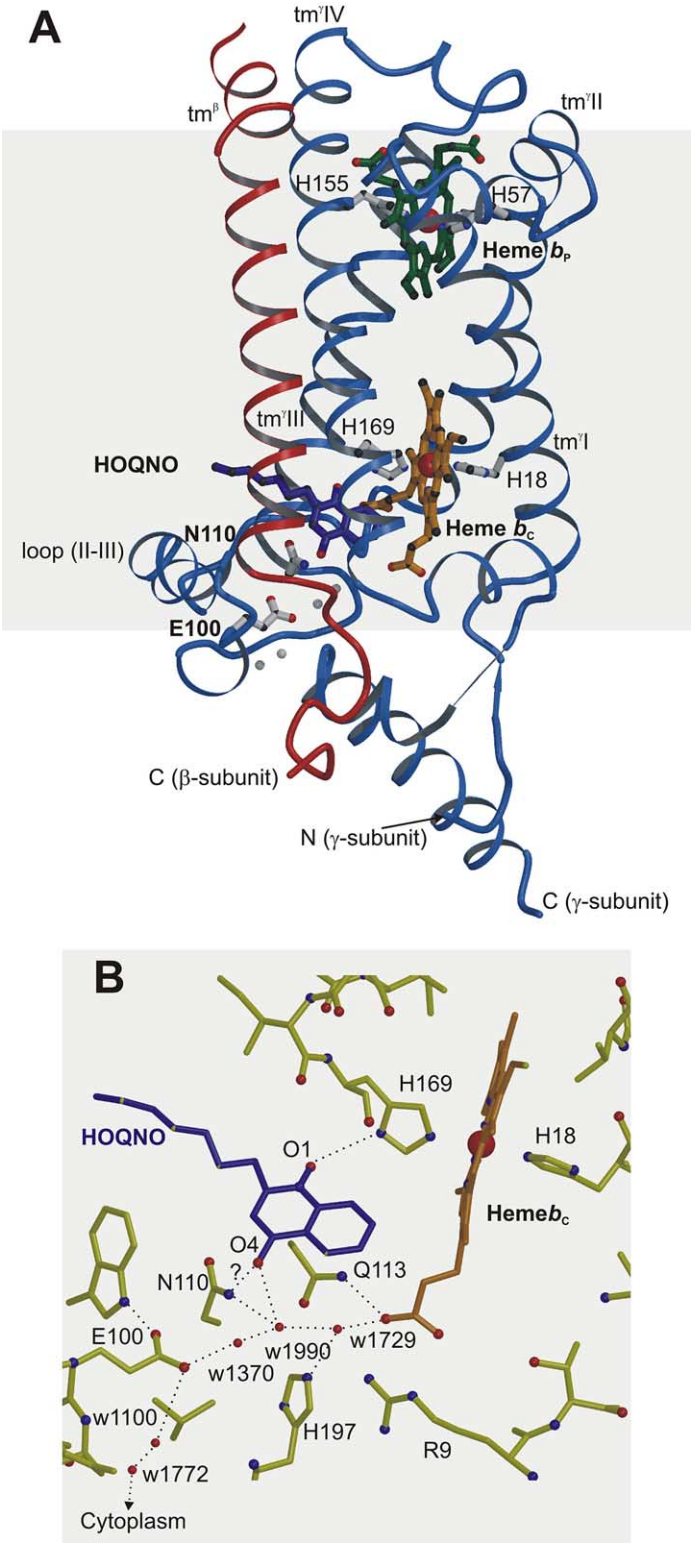


Fig. 3. Structure of the integral membrane domain of Fdh-N. A: View parallel to the membrane. Transmembrane helices for the γ-subunit are numbered from tm γ I to tm γ IV, and the one from the β-subunit is labeled as tm β. Residues involved in the binding of the two heme *b* groups and the HOQNO are also shown. Red dots correspond to water molecules involved in a possible proton pathway from the cytoplasm to the menaquinone binding site. B: Menaquinone binding site and water molecules in a possible proton pathway. This figure was made using MOLSCRIPT [34] and rendered using RASTER3D [35].

of HOQNO, the water chain connects the OH group (equivalent to $O_4$ of menaquinone) with the cytoplasmic space. We believe that this is the proton pathway to the menaquinone binding site.

## 5. PMF generation mechanism in the Fdh-N/Nar system

Thus, the HOQNO-inhibited structure revealed the menaquinone reduction site at the cytoplasmic side of the mem-

brane, compared to the location of the menaquinol oxidation site of Nar at the periplasmic side. Support for the quinol oxidation site being located on the periplasmic side of Nar comes from the observation that electron donation by the membrane-impermeable diquat radical is blocked by the quinol analog HOQNO [19]. Also, the redox potentials of the two heme *b*s of *E. coli* Nar were estimated in partially purified enzyme to be (at pH 7.0) +10 and 125 mV [30]. The lower-potential heme has a reduction potential close to that of the relevant quinone/quinol couple, consistent with this heme being the initial electron acceptor from quinol at the periplasmic face of the membrane. If the high-potential heme is situated on the cytoplasmic side of the membrane, then the potential difference between the heme *b*s could provide some of the work required to move the electrons against the transmembrane electrochemical potential (150–200 mV).

As mentioned earlier, the $H^+/e^-$ ratios differ for the enzymes and pathways induced. The ratio is also dependent on the topology of the enzymes. Fdh-N can couple the redox reaction to the reported proton translocation ($H^+/e^- = 1$) by the orientation of the substrate sites for formate and menaquinone [19,21]. Similarly, Nar yields an $H^+/e^- = 1$ ratio during menaquinol oxidation [19,31,32]. This can be compared to the menaquinol:fumarate reductase, which has an $H^+/e^-$ ratio of 0 due to the arrangement of the substrate sites. Proton release during menaquinol oxidation and proton consumption during fumarate reduction both take place on the cytoplasmic side of the membrane [33].

The Fdh-N structure, in combination with the Nar topology information and mutation analysis, demonstrates that Fdh-N and Nar generate PMF by the redox loop mechanism. In this respiratory pathway, two electrons are transferred from the formate oxidation site in the periplasm to the $NO_3^-$ reduction site in the cytoplasm. In the process, two protons are taken up from the cytoplasm at the Fdh-N menaquinone reduction site, and translocated across the membrane and released to the periplasm from the menaquinol oxidation site in Nar. This follows the principles in Mitchell's original chemiosmotic theory.

## 6. Outlook

There is a large quantity of biochemical and mutational data for the second enzyme in the pathway, Nar. However, to date no structural data are available. The final piece in the puzzle will fall into place when the structure of Nar is revealed, providing the definitive proof of Mitchell's redox loop mechanism almost 40 years after he first formulated his theory and 25 years after he won the Nobel prize for his seminal work.

*Acknowledgements:* This work has been supported by Biotechnology and Biological Sciences Research Council (BBSRC).

## References

[1] Mitchell, P. (1961) Nature 191, 144–148.
[2] Mitchell, P. (1966) Chemiosmotic Coupling in Oxidative and Photosynthetic Phosphorylation, Glynn Research, Bodmin, Cornwall.
[3] Tsukihara, T., Aoyama, H., Yamashita, E., Tomizaki, T., Yamaguchi, H., Shinzawa-Itoh, K., Nakashima, R., Yaono, R. and Yoshikawa, S. (1995) Science 269, 1069–1074.
[4] Iwata, S., Ostermeier, C., Ludwig, B. and Michel, H. (1995) Science 376, 660–669.
[5] Iwata, S., Lee, J.W., Okada, K., Lee, J.K., Iwata, M., Rasmussen, B., Link, T.A., Ramaswamy, S. and Jap, B.K. (1998) Science 281, 64–71.
[6] Yankovskaya, V., Horsefield, R., Tornroth, S., Luna-Chavez, C., Miyoshi, H., Leger, C., Byrne, B., Cecchini, G. and Iwata, S. (2003) Science 299, 700–704.
[7] Abrahams, J.P., Leslie, A.G., Lutter, R. and Walker, J.E. (1995) Nature 370, 594–595.
[8] Nicholls, D.G. and Ferguson, S.J. (1992) Bioenergetics 2, Academic Press, London.
[9] Richardson, D.J. (2000) Microbiology 146, 551–571.
[10] Unden, G. and Bongaerts, J. (1997) Biochim. Biophys. Acta 1320, 217–234.
[11] Berg, B.L. and Stewart, V. (1990) Genetics 125, 691–702.
[12] Stewart, V. (1988) Microbiol. Rev. 52, 190–232.
[13] Craske, A. and Ferguson, S.J. (1986) Eur. J. Biochem. 158, 429–436.
[14] Ballard, A.L. and Ferguson, S.J. (1988) Eur. J. Biochem. 174, 207–212.
[15] Berks, B.C., Page, M.D., Richardson, D.J., Reilly, A., Cavill, A., Outen, F. and Ferguson, S.J. (1995) Mol. Microbiol. 15, 319–331.
[16] Sawers, G., Heider, J., Zehelein, E. and Bock, A. (1991) J. Bacteriol. 173, 4983–4993.
[17] Berg, B.L., Li, J., Heider, J. and Stewart, V. (1991) J. Biol. Chem. 266, 22380–22385.
[18] Garland, P.B., Downie, J.A. and Haddock, B.A. (1975) Biochem. J. 152, 547–559.
[19] Jones, R.W., Lamont, A. and Garland, P.B. (1980) Biochem. J. 190, 79–94.
[20] Ingledew, W.J. and Poole, R.K. (1984) Microbiol. Rev. 48, 222–271.
[21] Jormakka, M., Tornroth, S., Byrne, B. and Iwata, S. (2002) Science 295, 1863–1868.
[22] Dias, J.M., Than, M.E., Humm, A., Huber, R., Bourenkov, G.P., Bartunik, H.D., Bursakov, S., Calvete, J., Caldeira, J., Carneiro, C., Moura, J.J., Moura, I. and Romao, M.J. (1999) Struct. Fold. Des. 7, 65–79.
[23] Boyington, J.C., Gladyshev, V.N., Khangulov, S.V., Stadtman, T.C. and Sun, P.D. (1997) Science 275, 1305–1308.
[24] Page, C.C., Moser, C.C., Chen, X. and Dutton, P.L. (1999) Nature 402, 47–52.
[25] Blasco, F., Guigliarelli, B., Magalon, A., Asso, M., Giordano, G. and Rothery, R.A. (2001) Cell. Mol. Life Sci. 58, 179–193.
[26] Rothery, R.A., Magalon, A., Giordano, G., Guigliarelli, B., Blasco, F. and Weiner, J.H. (1998) J. Biol. Chem. 273, 7462–7469.
[27] Taniguchi, S., Sato, R. and Egami, F. (1956) in: The Enzymatic Mechanisms of Nitrate and Nitrite Metabolism in Bacteria. A Symposium on Inorganic Nitrogen Metabolism; Function of Metallo-flavoproteins (McElroy, W.D. and Glass, B., Eds.), pp. 87–108, Johns Hopkins University Press, Baltimore, MD.
[28] Enoch, H.G. and Lester, R.L. (1975) J. Biol. Chem. 250, 6693–6705.
[29] Gross, R., Simon, J., Lancaster, C.R. and Kröger, A. (1998) Mol. Microbiol. 30, 639–646.
[30] Hackett, N.R. and Bragg, P.D. (1983) J. Bacteriol. 154, 708–718.
[31] Garland, P.B., Downie, J.A. and Haddock, B.A. (1975) Biochem. J. 152, 547–559.
[32] Morpeth, F.F. and Boxer, D.H. (1985) Biochemistry 24, 40–46.
[33] Geisler, V., Ullmann, R. and Kröger, A. (1994) Biochim. Biophys. Acta 1184, 219–226.
[34] Kraulis, J.P. (1991) J. Appl. Crystallogr. 24, 946–950.
[35] Merritt, E.A. and Murphy, M.E.P. (1994) Acta Crystallogr. Sect. D 50, 869–873.